Atmospheric Environment 252 (2021) 118323

Contents lists available at ScienceDirect

Atmospheric Environment

journal homepage: http://www.elsevier.com/locate/atmosenv

Assessing local emission for air pollution via data experiments

Yuru Zhu [a], Yinshuang Liang [b], Song Xi Chen [a,c,*]

[a] Center for Statistical Science, Peking University, Beijing, 100871, China
[b] School of Information Engineering, Zhengzhou University of Technology, Henan, 450044, China
[c] Guanghua School of Management, Peking University, Beijing, 100871, China

HIGHLIGHTS

- Calm periods after sustained cleaning processes are selected to gauge local emissions.
- Reductions in hourly growth rates of $PM_{2.5}$ and SO_2 were significant but less for NO_2 over years.
- Beijing's growth rates of $PM_{2.5}$ and NO_2 were comparable to the heavy industrialized Tangshan and Baoding.

GRAPHICAL ABSTRACT

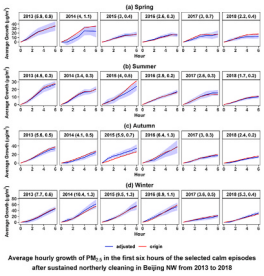

Average hourly growth of $PM_{2.5}$ in the first six hours of the selected calm episodes after sustained northerly cleaning in Beijing NW from 2013 to 2018

ARTICLE INFO

Keywords:
Air-quality assessment
Calm episodes
Meteorological adjustment
Panel data regression
Quasi-experiment

ABSTRACT

Although air pollution is largely due to anthropogenic emission, the observed pollution levels in a city are confounded by meteorological conditions and regional transportation of pollutants. However, effective air quality management requires measures for local emissions of the city. With a data selection algorithm, we choose calm episodes after strong cleaning processes to measure the growth of three air pollutants ($PM_{2.5}$, NO_2 and SO_2) before the arrival of transported pollution in three North China cities. Panel data regression models are used to analyze the episode data from the quasi-experiments to quantify the local emission in three North China cities from March 2013 to February 2019. The study reveals significant reductions in the average hourly growth rates from 5.9 to 11.1 $\mu g/m^3$ to 2.9–4.5 $\mu g/m^3$ for $PM_{2.5}$, 2.2–8.9 $\mu g/m^3$ to 0.4–2.5 $\mu g/m^3$ for SO_2 from 2013 to 2018, respectively, mounting to 44–70% and 57–82% reductions in the two pollutants in the three cities. However, the hourly growth rate for NO_2 was less changed with the annual decrease ranging from −9.4% to 27.9% over the 2013 level in 2018. The study also finds the growth rates of $PM_{2.5}$ and NO_2 in Beijing were comparable to those in the heavy industrialized Tangshan and Baoding, revealing Beijing's substantial emission despite its very low profile on SO_2.

1. Introduction

Air pollution is an environmental and public health issue in many countries, which is largely driven by excessive emissions due to anthropogenic activities. The purpose of air quality management is surely to reduce the emissions leading to air pollution. However,

* Corresponding author. Guanghua School of Management, School of Mathematical Science and Center for Statistical Science, Peking University, Beijing, 100871, China.
E-mail addresses: yuruzhu@pku.edu.cn (Y. Zhu), pingzi2000@126.com (Y. Liang), csx@gsm.pku.edu.cn (S.X. Chen).

https://doi.org/10.1016/j.atmosenv.2021.118323
Received 25 December 2020; Received in revised form 28 February 2021; Accepted 2 March 2021
Available online 17 March 2021

quantifying the amount of emissions including both anthropogenic and natural emissions in a city or a small area is a challenging task. Emission inventory (EI) is a tool for accounting for the amount of air pollutants discharged into the atmosphere from various pollution sources in a certain time span and a geographical area, which involves both the bottom-up approach that collects the amount of emissions from all sources of an area over a time frame and the down-scaling larger area production and energy statistics to smaller geographical areas (Bun et al., 2018; Gurney et al., 2012; Huang et al., 2015). The inventory is usually compiled every 3–4 years which implies temporal delays in using it for emission measurements, and is also subject to measurement errors. A Bayesian inverse model is used as a top-down method to infer the most likely distribution of emissions where bottom-up inventories are prior estimates and then updated using observed concentrations and an atmospheric transport model (Kunik et al., 2019; Nickless et al., 2018; Turnbull et al., 2019).

Air quality monitoring networks established in many countries in the last two decades provide data with a good spatial and temporal resolution, which may be used to gauge the emission. However, as the ground measurements of the pollution concentration from the monitoring sites are inevitably confounded by the meteorological conditions and regional transportation, obtaining emission information from the monitoring data requires data analytic techniques and proper study designs to filter out the meteorological effect and regional transportation. This paper provides one such technique. Although the measured concentration is generally positively correlated with the emission amount, it is not easy to estimate the underlying emission by inverting the concentrations, as meteorological factors can confound the concentration levels, the same level of emission with different meteorological conditions can lead to different concentrations at the monitoring sites. Liang et al. (2015) and Zhang et al. (2020) provided statistical adjustments to the observed concentrations under a standardized weather baseline so that the adjusted concentrations are comparable temporally (Liang et al., 2015) and spatially (Zhang et al., 2020), which under certain conditions can be used as indications of the overall emission. However, in addition to the meteorological confounding, regional transportation is another factor that is not accounted for in the meteorological adjustment approach. This was the motivation to study the monitoring data over calm periods after each refreshment of the air quality.

Studies have shown air quality is much influenced by meteorology and regional transportation. Regional transport of pollutants was found to contribute to concentrations of $PM_{2.5}$ (Wang et al., 2014b, c; Zheng et al., 2015) and SO_2 (Yang et al., 2013) in Beijing. Huang et al. (2014) and Wang et al. (2014a) showed that certain wind and humidity conditions were related to high $PM_{2.5}$ concentrations in Beijing. Seo et al. (2017) investigated a severe haze episode in 2014 at both an urban site in Seoul and an upwind background site on Deokjeok Island, and found warm, humid and stagnant meteorological conditions were conducive to the accumulation of pollutants and the oxidation of precursors. Su et al. (2017) found a dilution effect on the pollution by the planetary boundary layer height (BLH) which defines the aerosol vertical conditions. Su et al. (2018) conducted an analysis of the BLH and $PM_{2.5}$ concentrations over four major regions of China, and concluded that BLH was largely negatively correlated with the particulate matter concentration. An adjustment approach to removing meteorological confounding in the observed concentrations was proposed in (Liang et al., 2015; Zhang et al., 2020) via the nonparametric regression model and constructing a baseline meteorological distribution.

Numerical models have been constructed to account for pollutant concentrations, the meteorological and chemical processes, as well as their interactions on regional air quality, such as the Community Multi-Scale Air Quality (CMAQ), the Comprehensive Air Quality Model with extensions (CAMx), the PSU/NCAR Mesoscale Model (MM5) and the Weather Research and Forecast (WRF)-Chem model; see Wang et al. (2014b); Xing et al. (2011) and Li et al. (2015); Titov et al. (2007); Wu et al. (2013) and Lee et al. (2009) and Tie et al. (2007) for applications in air quality assessment. The numerical models can evaluate the effectiveness of control measures via simulating different emission control scenarios. In the CAMx model, Particulate Source Apportionment Technology (PSAT) which is a source tagging method can track the relative source contribution to pollutant concentrations (Li et al., 2015). Chen et al. (2019) employed a combined CAMx, WRF, the source emission model (SMOKE) to evaluate two pairs of pollution episodes each of which happened in different years but had similar meteorological conditions and found a dramatic decrease in SO_2 over the years with nitrate ions being the dominant $PM_{2.5}$ component. The relative contribution of coal combustion to $PM_{2.5}$ concentrations in Beijing dropped from 40% in March 2013 to 11% in March 2018 as a result of China's "Coal to Gas" project and "2 + 26 Cities" regional air quality management strategy (MEP, 2017). Huang et al. (2017) compiled and analyzed a global NO_x emission inventory to explore spatial and temporal trends in emissions from 1960 to 2014, which suggested a dramatic increase in annual anthropogenic emissions of NO_x from 7.39 to 67.8 Tg in developing countries and showed slow progress on NO_x emission control.

In the last two decades, live air quality monitoring data are increasingly available to provide timely measurements on a set of pollutants in many locations in the world. However, the data may not entirely reflect emission at a location because they are influenced by regional transportation and meteorological conditions as shown above. As revealed in Liang et al. (2015) and Zhang et al. (2017), the air quality in the North China Plain (NCP) is governed by the northerly versus southerly wind regimes. This is largely due to the north and northwest of NCP is either the mountainous region or semi-arid grass and farming land with much less population and industrial loading as compared to those in the NCP, while the NCP and especially south of the NCP is fully installed with heavy industrial activities and high population density (Zheng et al., 2015). North China is governed by a periodic strong gale from Siberia which generates strong northerly wind that sweeps through the NCP and refreshes the air quality in the region.

Therefore, the cleaning processes in the NCP are typically conducted by strong northerly winds that blow away the pollutants and refresh the near earth atmosphere, while southerly wind brings more polluted air mass from the southern part of the NCP.

Motivated by the geographical and meteorological reality in the NCP, we develop an algorithm to select temporal segments of the time series observations corresponding to calm periods (calm episodes) after sustained northerly cleaning but before the arrival of the transported pollutants for three cities: Beijing, Tangshan and Baoding in the northern part of NCP. Indeed, every time after a strong northerly system thoroughly refreshes the air, it offers an opportunity to check on the growth of air pollution in a city over a period of calm weather before transported pollutants are brought by the unfavorable winds. By applying seasonal regression for panel data with hourly dummy variables, the hourly growth rates of three pollutants ($PM_{2.5}$, SO_2 and NO_2) from the start of the calm episodes are estimated. To remove meteorological confounding, the estimated growth rates are adjusted according to the meteorological baseline distributions based on data from 2013 to 2018. The analysis reveals a sustained reduction trend in the adjusted average growth rates of $PM_{2.5}$ and SO_2 since 2013. However, the NO_2 growth rates had not been reduced significantly in the two Hebei cities with some notable increases over the years, and for Beijing there were only some signs of reduction emerging in 2017 and 2018. These reflect the air quality management strategy in North China which has been much focused on improving the coal related emission and control, while the vehicle related emission controls are much lagged behind those for coal consumption.

2. Data and variables

The air pollution data analyzed in this study are hourly concentrations from the so-called Guokong monitoring sites in three North China

cities: Beijing, Baoding and Tangshan. The Guokong sites are directly administrated by China's Ministry of Ecology and Environment (MEE) to avoid potential local interference. We focus on the hourly $PM_{2.5}$, SO_2 and NO_2 concentrations during the selected calm episodes from six sites in Beijing, three sites in Baoding and Tangshan, respectively. Among the six Guokong sites in Beijing, there are two clusters of sites with each having three sites. One cluster is located in the northwest (hence Beijing NW), and another in the southeast (Beijing SE) of central Beijing. Tangshan is a steel-making city 155 km (KMs) to the east of Beijing, and Baoding is 140 KMs southwest of Beijing. Figure S1 of the supporting information (SI) provides a map on the northern portion of the NCP that encompasses the three cities, and Table S1 has details on the site clusters in the three cities. To reduce measurement errors, we applied a five point moving average filter over the hourly time series data with weights 0.1, 0.2, 0.4, 0.2 and 0.1 for $t-2, t-1, t, t+1$ and $t+2$, respectively.

We matched each of the air quality monitoring clusters in the three cities with the nearest meteorological station from China Meteorological Administration (CMA). Specifically, two CMA stations are employed in Beijing, one for Baoding and Tangshan, respectively, as shown in Table S1. The meteorological variables include hourly measurements of the dew point temperature (DEWP), relative humidity (HUMI), air pressure (PRES) and temperature (TEMP), wind direction (W) and speed (WS), cumulative wind speed (CWS) and precipitation (R). The wind directions are grouped into five categories based on the study of Liang et al. (2015): northeast (NE) having NNE, NE and ENE (according to the azimuth degrees on the rose wind plot); northwest (NW) for W, WNW, NW, NNW and N; southeast (SE) including E, ESE, SE, SSE and S; southwest (SW) having SSW, SW and WSW; and CV for the calm and variable wind. The CWS at time t sums over wind speed from the first hour of a wind direction to time t under the same wind direction. Whenever there is a change of direction, it is set to zero and starts to accumulate under the new direction. Furthermore, we define the cumulative northerly (southerly) wind speed CNWS (CSWS) that merges NE and NW (SE and SW).

We obtained hourly boundary layer dissipation (BLD) and boundary layer height (BLH) from the Global Reanalysis data ERA5 provided by the European Center for Medium-Range Weather Forecasts (ECMWF) at a grid resolution of 0.5×0.5 (latitude by longitude). The grid location of the ERA5 data stream which was closest to the center of the air quality monitoring clusters was used for the site cluster. We took the logarithm of humidity (LogHUMI), boundary layer dissipation (LogBLD) and boundary layer height (LogBLH) to reduce the skewness of the measurements. Furthermore, we composed two pre-episode variables: the sum of hourly northerly wind speed (SNWS) and the maximum of the cumulative northerly wind speed (MCNWS) in the 24 h before the calm episodes. These two variables reflected the extent of northerly cleaning.

The time range of the study is from March 2013 to February 2019 which spans over six seasonal years, where one seasonal year covers spring (March to May), summer (June to August), fall (September to November), and winter (December to February next year), and the season is the basic unit of analysis.

Figure S2 shows $PM_{2.5}$ versus the accumulated wind speed under five wind directions in four seasons in 2015 for the four site clusters. Patterns of the wind effects for other years are similar. The figure shows strong cleaning effects of the northerly winds while such effects can not be seen for southerly winds in three cities. Figure S3 reports pair-wise Spearman's rank correlation coefficients between the three pollutants ($PM_{2.5}$, SO_2 and NO_2) and the cumulative northerly (CNWS) and southerly (CSWS) wind speeds in 2015 for the four site clusters, which confirms Figure S2's revelation. The only exception is for NO_2 in the summer and the southerly wind's effect in Baoding in winter. The latter is because Baoding is closer to the middle of the NCP, where the effect of the northerly cleaning is not as profound as in the other two cities located toward the northern edge of the NCP. In contrast, Beijing tends to be the first one among NCP cities to be scavenged by the northerly cleaning processes (Zheng et al., 2015), which makes the correlation more pronounced.

We write $\{WS_t\}_{t=1}^{L}$, $\{CNWS_t\}_{t=1}^{L}$ and $\{CSWS_t\}_{t=1}^{L}$ for time series of the instantaneous wind speed, the cumulative northerly and southerly wind speed, respectively, $\{R_t\}_{t=1}^{L}$ for the cumulative precipitation, and $\{PM2.5_t\}_{t=1}^{L}$ for concentrations of $PM_{2.5}$. Here L is the total length of observation time in a season for a site cluster.

3. Calm episodes

The selection of calm episodes for gauging local emissions consists of identifying three key time points: (i) the ending time t_ω of northerly cleaning processes, (ii) the beginning time t_s and (iii) the ending time t_e of the calm episodes. We first define $\mathscr{A}$ to be the set of ending times t_ω of northerly cleaning processes, which satisfy

$$\mathrm{CNWS}_{t_\omega-1} \geq 10.8\mathrm{m/s} \text{ and } \mathrm{CNWS}_{t_\omega} = 0. \tag{3.1}$$

It is noted that $\mathrm{CNWS}_{t_\omega} = 0$ implies a change of wind direction from the northerly, and 10.8 m/s (meters/second) corresponds to the lower limit of a strong breeze at grade 6 on the Beaufort scale. As it is the cumulative northerly wind, it would not be restrictive. It is noted that Beaufort scale is usually for instantaneous wind. Our use here is to decide proper cut-off levels for different classes of the cumulative winds under a direction. The Beaufort scale is the most relevant scale for that purpose.

We then locate the starting time t_s of a calm episode around each $t_\omega \in \mathscr{A}$, which corresponds to the lowest $PM_{2.5}$ in a neighborhood of t_ω (an 8-h window before and after t_ω) within a calm, cleaned and dry period, as the purpose of the study is to investigate $PM_{2.5}$ growth characteristics after cleaning by the northerly but before the transported pollution under the southerly wind. Imposing the dryness condition is to avoid mixing the cleaning due to the northerly wind and that by precipitation. As North China is generally dry in the non-summer seasons, the dryness requirement is also not restrictive.

Let $\mathscr{C}$ be the set of times when the system is calm, clean and dry satisfying

$$\mathrm{WS}_t \leq 5.4\mathrm{m}/\mathrm{s}, \max\{\mathrm{PM2.5}_{t-1}, \mathrm{PM2.5}_t\} \leq 35\mu\mathrm{g}/\mathrm{m}^3, \mathrm{R}_{t-1} = \mathrm{R}_t = 0, \tag{3.2}$$

where the wind speed (WS_t) is confined to grades 0–3 (no more than 5.4 m/s) on the Beaufort wind scale. It requires that $PM_{2.5}$ is not larger than $35\mu g/m^3$ for two consecutive hours, where $35\mu g/m^3$ is the daily threshold level for acceptable air quality in China. We replace $35\mu g/m^3$ with $50\mu g/m^3$ for Tangshan and Baoding due to more severe baseline pollution in the two cities because of heavier industrial installations in the two cities. Using the higher threshold was to ensure enough sample sizes for the selected calm episodes in the two cities. To gain information on the effects of the thresholds, Table S2 reports the number of the selected calm episodes and the associated statistics with the baseline being 35, 40 and 50 $\mu g/m^3$, respectively. Table S2 shows that at least 70% of the selected episodes under the 50 $\mu g/m^3$ were also chosen at the 35 $\mu g/m^3$ baseline, which implies that the results under the two baseline levels would be consistent. However, it shows using the threshold at 35 would reduce the number of the episodes beginning during the day for Baoding in summer and fall by 4/14 and 3/13 respectively, and Tangshan in autumn by 3/20, and would increase the variation of the estimation.

Let $\mathscr{E}_{t_\omega}$ be the set of the ending times of the previously selected calm episodes that ends before t_ω. It starts as an empty set $\mathscr{E}_0 = \varnothing$ and is updated by adding the ending times of selected calm episodes. The start time t_s of a new episode is obtained by searching within an 8-h neighborhood of t_ω within $\mathscr{C}$ after the ending time of the previous episode, namely

$$t_s = \arg\min_{t \in \mathscr{B}_{t_\omega}} \mathrm{PM2.5}_t, \tag{3.3}$$

where $\mathscr{B}_{t_\omega} = [t_\omega - 8, t_\omega + 8] \cap (max\{t : t \in \{0\} \cup \mathscr{E}_{t_\omega}\}, L] \cap \mathscr{C}$. Due to the atmospheric variation and measurement errors, t_s and t_ω may not coincide as the cleaning processes can stop before or continue after t_ω. Table 1 reports the seasonal averages for $t_s - t_\omega$ for each site cluster, which shows that t_s tended to be earlier than t_ω with the average differences to be the largest in winter in Beijing NW at −2.5 h (SE 0.1) and Beijing SE -2.2 (0.1), while the differences in the other sites and seasons were milder.

After attaining a t_s, we monitor the calm episodes starting from t_s until

$$\mathrm{R}_t = 0, \mathrm{CNWS}_t \leq 3.3\mathrm{m/s} \quad \text{and} \quad \mathrm{CSWS}_t \leq 13.8\mathrm{m/s} \tag{3.4}$$

is not satisfied. The last hour such that Condition (3.4) is satisfied is the episode's ending time t_e. Condition (3.4) excludes continuous cleanings by the northerly or substantial transportation by the southerly wind, respectively. It is noted that 3.3 m/s and 13.8 m/s correspond to Beaufort wind force at Grades 2 and 6, respectively. Grade 6 may look strong. However, it is the cumulative wind over previous hours, hence it is not that restrictive.

We filtered out episodes whose length ($t_e - t_s$) is less than 3 h to avoid short and unstable episodes. The algorithm for the calm episode selection is described in Algorithm 1 in the SI. The selected episodes in the winter of 2013 in Beijing's Dongsi site are shown in Fig. 1 against the overall time series of $PM_{2.5}$ and the cumulative northerly or southerly wind speed (CNWS or CSWS), respectively. The average numbers of episodes and the summary statistics in the four site clusters are reported in Table 1. For clusters in Beijing and Tangshan, the number of calm episodes was largest in winter, followed by autumn, summer and spring, as northerly cleaning processes were more frequent in winter. The numbers of calm episodes in Baoding were less than those of the other two cities, which was largely because generally weaker northerly wind in Baoding as shown in panel (d) of Figure S2. Table 1 also shows that the majority of calm episodes happened during the day (6 a.m.-6 pm). For all the four site clusters, the average length of calm episodes was smallest in spring, which was around 7 h, due to more air turbulence in the more windy spring season in that part of China. It is noted that we select the calm episodes after substantial northerly cleaning separately for each city. Each city would have experienced the cleaning before the calm episodes, which should avoid the potential transportation among the four site clusters. Also, wind is only one aspect of the conditions, and we also check on $PM_{2.5}$ level to control for the regional transportation.

Figure S4 shows the seasonal distribution of $t_s - t_\omega$ for the selected calm episodes of each site cluster, while Figure S5 presents the radar plots that depict the distributions of the wind direction and speed 4 h before $\min\{t_s, t_\omega\}$ and 4 h after $\max\{t_s, t_\omega\}$, respectively, in spring of cluster Beijing SE. The wind distribution before $\min\{t_s, t_\omega\}$ is dominated by NW and NE, and by SW and SE during the 4 h after $\max\{t_s, t_\omega\}$. The period between t_s and t_ω saw a drop in NW in both percentage and velocity. Furthermore, Fig. 2 displays changes in the average meteorological variables in the 4 h before and after the start of the calm episodes for cluster Beijing NW in each season. Similar figures for the other three clusters are provided in Figures S6 – S8. In general, we can find a common downward trend in BLD, BLH, TEMP and CNWS and an upward trend in DEWP, HUMI and CSWS after the starting of the calm episodes. These characteristics are related to the build-up of pollutants in the calm episodes, which is in line with the conclusions in the existing literature about the effects of meteorological conditions on pollutant concentrations (Liang et al., 2015; Zheng et al., 2015). From Figure S9 we can find that the patterns of concentrations for $PM_{2.5}$, SO_2 and NO_2 during the episodes beginning in the two time periods, day (6 a.m.-6 pm) and night (7 p.m.-5 am), are different. Meanwhile, more episodes happened in the day. Therefore, we only consider comparing the results of episodes which started between 6 a.m. and 6 p.m. for better control of hidden factors.

4. Methods

4.1. Models for calm episodes

As shown in Table 1, the average length of the gap time between consecutive episodes was at least 60 h in all seasons, and that in the non-winter seasons was even longer. Hence, different episodes may be regarded as independent, which leads us to consider a linear model for the growth of the pollutants during the episodes. It is noted that the sites within a cluster are quite close to each other, thus data from the three air-quality monitoring sites in a cluster are pooled to fit a common model for a season to make the analysis robust.

For a site cluster and a season, at an hour t in the j-th episode of year i, let Y_{ijt} be the concentration of a pollutant ($PM_{2.5}$, NO_2 or SO_2), $C_{ij} = (\mathrm{SNWS}_{ij}, \mathrm{MCNWS}_{ij})^\top$ be the two pre-episode variables, and

Table 1
Summary statistics of selected calm episodes in four different clusters from March 2013 to February 2019, including the average number and the average numbers of episodes which began during the Day (6 a.m.-6 pm) and at the Night (7 p.m.-5 am) for each season in one site and one year, the average, 25%, 50% and 75% quantiles of the Length of the episodes, the average Range (the difference between the maximum and minimum $PM_{2.5}$ in the calm episode, $\mu g/m^3$), the average $t_s - t_\omega$ (hours) between the episode's start and the ending time t_ω of a northerly cleaning process and the average Gap Time (hours) between two consecutive episodes with the standard error in the parentheses.

Cluster	Season	Count	Day	Night	Length				$PM_{2.5}$ Range	$t_s - t_\omega$	Gap Time
					Average	Q1	Q2	Q3			
Beijing SE	spring	16	11	5	7.4 (0.3)	4	6	9	33 (2.2)	−1.5 (0.2)	122.9 (7.9)
	summer	19	15	4	7.8 (0.2)	5	7	10	25.7 (1.3)	−0.5 (0.2)	106.3 (6)
	autumn	24	20	4	9.2 (0.2)	6	8	12	33.6 (1.3)	−1 (0.1)	80.2 (3.4)
	winter	27	23	4	9.3 (0.2)	6	9	12	62.6 (2.5)	−2.2 (0.1)	67 (2.4)
Beijing NW	spring	16	11	5	7.6 (0.2)	4	7	10	31.8 (1.8)	−1.2 (0.2)	124.8 (6.1)
	summer	19	15	4	9.5 (0.3)	5	9	12	26.2 (1.2)	−0.7 (0.2)	103.2 (5.7)
	autumn	23	18	5	10.7 (0.3)	6	10	13	32.2 (1.4)	−1.1 (0.2)	82.8 (3.6)
	winter	25	22	3	9.7 (0.2)	7	9	12	56.1 (2.4)	−2.5 (0.1)	74.7 (3.2)
Tangshan	spring	19	14	5	6.9 (0.2)	4	6	9	37.2 (1.6)	−1.5 (0.2)	101.4 (5.3)
	summer	17	10	7	8.5 (0.3)	5	8	12	31 (1.5)	−0.2 (0.2)	114.3 (7.5)
	autumn	25	20	5	10.5 (0.3)	6	10	14	45.8 (2)	−1.6 (0.1)	71.1 (3.6)
	winter	30	24	6	9.2 (0.2)	5	8	12	56.1 (2.1)	−1.9 (0.1)	61.8 (2.9)
Baoding	spring	16	11	5	7.9 (0.3)	4	6	10	38 (2.3)	−0.6 (0.2)	122.2 (6.9)
	summer	21	14	7	9.6 (0.3)	5	8	12	35.1 (2.1)	−0.7 (0.2)	91.4 (4.9)
	autumn	16	13	3	13 (0.5)	7	12	18	54.7 (3.7)	−0.6 (0.2)	109.1 (4.7)
	winter	18	14	4	11.1 (0.4)	5	9	17	70.7 (3.7)	−0.9 (0.2)	107.6 (7.2)

Fig. 1. The time series of $PM_{2.5}$ ($\mu g/m^3$), cumulative northerly wind speed (green) and cumulative southerly (purple) wind speed (m/s) in winter of 2013 in Dongsi with observations of $PM_{2.5}$ during the calm episode shown in red, otherwise in black. The gray and brown dashed lines mark 35 $\mu g/m^3$ and 10.8 m/s, respectively. (For interpretation of the references to color in this figure legend, the reader is referred to the Web version of this article.)

be the vector of eight meteorological variables, for $i = 1,\cdots,A, j = 1,\cdots$

$$\Delta Y_{ijt} = \Delta M_{ijt}^{\top}\beta_i + C_{ij}^{\top}\gamma_i + I_{ijt}^{\top}\eta_i + \varepsilon_{ijt}, \quad j = 1,\cdots,n_i \text{ and } t = 1,\cdots,T_{ij}, \tag{4.1}$$

$$M_{ijt} = \left(\mathrm{DEWP}_{ijt}, \mathrm{PRES}_{ijt}, \mathrm{TEMP}_{ijt}, \mathrm{LogBLD}_{ijt}, \mathrm{LogBLH}_{ijt}, \mathrm{LogHUMI}_{ijt}, \mathrm{CNWS}_{ijt}, \mathrm{CSWS}_{ijt}\right)^{\top}$$

$, n_i$ and $t = 0,\cdots,T_{ij}$. Here $A = 6$ is the total number of years in the study, n_i is the number of episodes in year i of the season in the site cluster, $t = 0$ corresponds to the starting time t_s of a calm episode defined in Section 3 and T_{ij} is the length of the j-th episode. Since the focus of the study is the pattern of pollution build-up in the episodes, we introduce a difference operator $\Delta A_{ijt} = A_{ijt} - A_{ij0}$ for a generic variable A. To reflect the hourly growth, we define $I_{ijt} = (I_{ijt}^1, I_{ijt}^2, \cdots, I_{ijt}^{T_{ij}})^{\top}$ of dummy variables for $1, 2, \cdots, T_{ij}$ hours after the episode starts for the time-effect. Then the model in year i for the longitudinal (panel) data in a cluster of a season is

where ε_{ijt} are possibly heterogeneous random errors with zero conditional mean and finite conditional variance given the explanatory variables. Let $\theta_i = (\beta_i^{\top}, \gamma_i^{\top}, \eta_i^{\top})^{\top}$ be the $p \times 1$ vector of parameters, where p is the number of regressors. As the model parameters and their estimation are year, season and cluster specific, the year, season and cluster fixed effects are reflected in the parameters.

Model (4.1) allows heterogeneity and serial correlations in the error terms $\{\varepsilon_{ijt}\}_{t=1}^{T_{ij}}$ that can be detected by the residual plot or tests (Breusch and Pagan, 1979; Wooldridge, 2010). In this study we use the ordinary least squares (OLS) estimator for θ_i with the robust variance estimator to

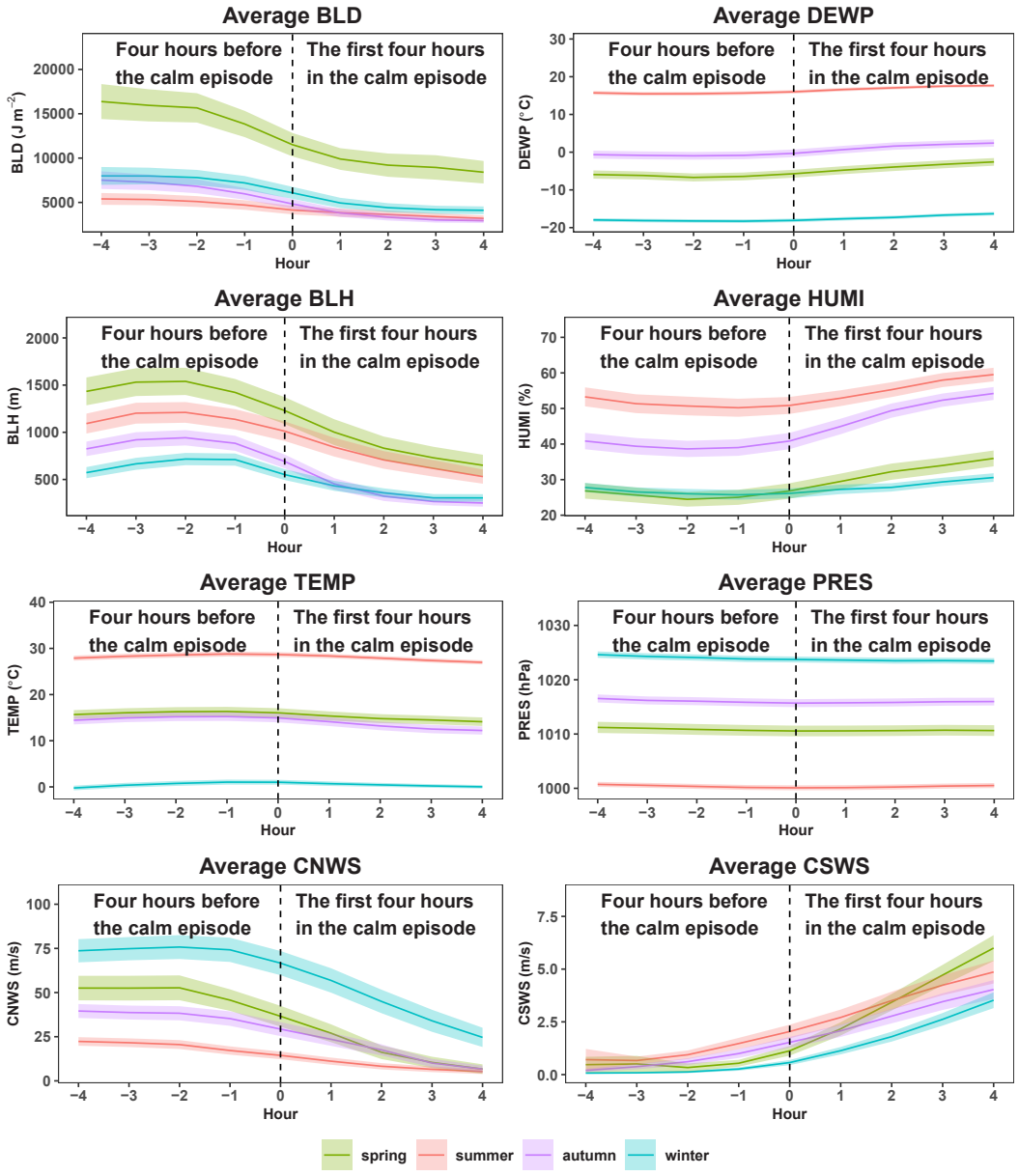

Fig. 2. The average boundary layer dissipation (BLD), dew point temperature (DEWP), boundary layer height (BLH), relative humidity (HUMI), temperature (TEMP), air pressure (PRES), cumulative northerly wind speed (CNWS), and cumulative southerly wind speed (CSWS) in the 4 h before and after the start of the calm episodes indicated by the dashed vertical line at zero in Beijing NW in spring (green), summer (red), autumn (purple) and winter (blue) with the 95% confidence intervals indicated by the colored areas. (For interpretation of the references to color in this figure legend, the reader is referred to the Web version of this article.)

avoid potential misspecifications on the dynamic structure of $\{\varepsilon_{ijt}\}_{t=1}^{T_{ij}}$ (Beck and Katz, 1995).

Let $\widetilde{T}_i = \max_j T_{ij}$ be the maximum length of the episodes in year *i*. As there are $\widetilde{T}_i + 10$ regressors in the panel regression, to avoid model overfitting, we first select the important variables by the forward step-wise method based on the Bayesian information criterion (BIC) (Hastie et al., 2008), which chooses one variable at each step that leads to the largest reduction in the BIC until none variable can be added to reduce the BIC. Since the length of the calm episodes varies, we regard the time dummies as a whole in the forward selection. See Xu et al. (2020) for a similar exercise. Table 2 reports the selected variables and their order of selection for $PM_{2.5}$ in spring.

It is shown that the time dummies were the most important one and were always selected first, and there was much accordance in the variable importance for the growth of a pollutant among different site clusters at a season. Table 3 summarizes the relative frequencies of the selected variables for the three pollutants in four seasons in 2013–2018. It shows that PRES, BLD and SNWS were key variables for the growth of $PM_{2.5}$ in the calm episodes with TEMP being also significant for the growth of $PM_{2.5}$ in autumn and winter. Besides, TEMP, BLH and HUMI were important for the growth of NO_2. As for the growth of SO_2, PRES and BLH were important with HUMI and MCNWS also selected frequently in autumn and winter. Table S3 presents the six-year average of the estimates for the year, season and cluster specific coefficients of selected variables in the model for each pollutant. All predictors have been standardized before the estimation so that the estimates are directly comparable, which confirms the importance of variables shown in Table 3 and implies a generally strong effect of TEMP and HUMI on pollutant concentrations as well as the negative effect of the pre-episode variable SNWS. It is noted that unlike the analyses with longer time series data (Liang et al., 2015; Xu et al., 2020), Table 2 shows much

Table 2
Variable ranks by the forward selection method for $PM_{2.5}$ in the spring of each year in different clusters during calm episodes and their average ranks, and the successive average R^2, AIC and BIC scores. A "-" indicates the selection was ended before the variable, which is given a rank of 11. The variables above the dashed line are those selected into the common baseline model according to the lowest average BIC.

Cluster	Variable	2013	2014	2015	2016	2017	2018	Average Rank	Average R^2	Average AIC	Average BIC
Beijing SE	Time dummies	1	1	1	1	1	2	1.2	0.68	1735	1800
	ΔDEWP	3	—	2	—	4	4	5.8	0.69	1713	1781
	MCNWS	—	4	—	—	3	1	6.8	0.72	1705	1777
	ΔLogBLH	—	—	—	2	2	5	7.0	0.75	1693	1768
	ΔLogHUMI	—	3	4	—	5	—	7.5	0.77	1682	1760
	SNWS	4	—	—	—	—	3	8.5	0.77	1681	1762
	ΔPRES	2	—	—	—	6	—	8.7	0.79	1659	1743
	ΔTEMP	—	—	—	3	—	6	8.8	0.81	1644	1732
	ΔLogBLD	—	2	—	—	7	—	8.8	0.81	1641	1732
	ΔCNWS	—	—	3	—	—	—	9.7	0.81	1642	1736
	ΔCSWS	—	—	5	—	—	—	10.0	0.82	1637	1735
Beijing NW	Time dummies	1	1	1	1	1	1	1.0	0.68	2145	2215
	ΔDEWP	2	—	4	—	3	2	5.5	0.71	2126	2199
	ΔLogBLD	3	—	5	4	5	6	5.7	0.72	2121	2197
	ΔPRES	—	4	2	—	—	4	7.2	0.73	2114	2193
	ΔTEMP	—	5	3	3	—	—	7.3	0.76	2085	2168
	ΔLogHUMI	4	6	—	—	—	3	7.7	0.77	2074	2161
	MCNWS	—	2	—	—	2	—	8.0	0.78	2071	2161
	ΔCNWS	—	3	—	—	6	7	8.2	0.79	2063	2157
	ΔCSWS	—	—	—	2	7	—	8.8	0.79	2058	2156
	SNWS	—	—	—	—	4	5	8.8	0.80	2058	2159
	ΔLogBLH	—	—	—	—	—	—	11.0	0.80	2059	2163
Tangshan	Time dummies	1	1	1	1	1	1	1.0	0.80	2401	2469
	ΔPRES	2	2	3	5	—	2	4.2	0.85	2327	2399
	ΔLogHUMI	7	4	—	2	4	—	6.5	0.85	2316	2391
	SNWS	4	5	—	—	5	5	6.8	0.86	2310	2389
	MCNWS	5	—	—	—	3	3	7.3	0.86	2300	2382
	ΔCSWS	—	—	—	4	2	6	7.5	0.87	2297	2383
	ΔDEWP	—	3	—	6	—	4	7.7	0.87	2283	2372
	ΔTEMP	6	—	2	—	—	—	8.7	0.88	2282	2375
	ΔLogBLD	3	6	—	—	—	—	8.8	0.88	2275	2372
	ΔLogBLH	—	—	—	3	—	—	9.7	0.88	2274	2374
	ΔCNWS	—	—	—	—	—	—	11.0	0.88	2273	2377
Baoding	Time dummies	1	1	1	1	1	1	1.0	0.81	2264	2341
	ΔPRES	—	2	3	—	2	2	5.2	0.83	2223	2303
	ΔLogHUMI	2	6	2	—	6	—	6.3	0.86	2157	2240
	ΔLogBLD	4	—	—	—	3	4	7.3	0.87	2148	2235
	ΔCSWS	5	—	—	5	7	5	7.3	0.87	2141	2231
	ΔLogBLH	—	5	—	4	—	3	7.5	0.88	2137	2231
	ΔTEMP	3	—	4	—	8	—	8.0	0.88	2133	2230
	ΔDEWP	—	—	5	2	9	—	8.2	0.89	2117	2218
	ΔCNWS	—	—	—	3	4	—	8.5	0.89	2107	2211
	SNWS	—	3	—	—	10	6	8.7	0.89	2102	2210
	MCNWS	—	4	—	—	4	—	8.0	0.89	2098	2206

Table 3
Relative frequencies of variables being selected within the first six steps of the forward selection procedure for the four seasons and three pollutants.

		(a)$PM_{2.5}$									
Spring	Time dummies	ΔLogHUMI	ΔPRES	ΔLogBLH	ΔLogBLD	SNWS	ΔCSWS	MCNWS	ΔDEMP	ΔTEMP	ΔCNWS
	1	1	0.75	0.5	0.5	0.5	0.5	0.5	0.5	0.25	0
Summer	Time dummies	ΔPRES	ΔLogBLD	ΔCSWS	SNWS	MCNWS	ΔDEMP	ΔTEMP	ΔLogHUMI	ΔLogBLH	ΔCNWS
	1	1	0.75	0.75	0.5	0.5	0.5	0.25	0.25	0.25	0.25
Autumn	Time dummies	ΔLogBLD	ΔTEMP	SNWS	ΔDEMP	ΔLogHUMI	ΔCSWS	ΔPRES	ΔLogBLH	ΔCNWS	MCNWS
	1	1	0.75	0.75	0.75	0.5	0.5	0.25	0.25	0.25	0
Winter	Time dummies	ΔTEMP	ΔLogBLD	SNWS	ΔPRES	ΔLogHUMI	ΔLogBLH	MCNWS	ΔDEMP	ΔCSWS	ΔCNWS
	1	1	0.75	0.75	0.5	0.5	0.5	0.5	0.5	0	0
	(b) NO_2										
Spring	Time dummies	ΔTEMP	ΔLogBLH	ΔPRES	ΔLogHUMI	SNWS	ΔLogBLD	ΔCSWS	MCNWS	ΔDEMP	ΔCNWS
	1	1	1	0.75	0.75	0.5	0.25	0.25	0.25	0.25	0
Summer	Time dummies	ΔTEMP	ΔLogHUMI	ΔCSWS	ΔPRES	ΔLogBLD	ΔCNWS	ΔLogBLH	SNWS	MCNWS	ΔDEMP
	1	1	1	0.75	0.5	0.5	0.5	0.25	0.25	0.25	0
Autumn	Time dummies	ΔLogHUMI	ΔLogBLH	ΔTEMP	ΔLogBLD	ΔPRES	ΔCNWS	ΔCSWS	MCNWS	SNWS	ΔDEMP
	1	1	1	0.75	0.75	0.5	0.5	0.25	0.25	0	0
Winter	Time dummies	ΔTEMP	ΔLogBLH	ΔLogBLD	ΔLogHUMI	SNWS	ΔCSWS	ΔPRES	MCNWS	ΔDEMP	ΔCNWS
	1	1	0.75	0.75	0.5	0.5	0.5	0.25	0.25	0.25	0.25
	(c)SO_2										
Spring	Time dummies	ΔPRES	ΔTEMP	ΔLogBLH	ΔLogHUMI	SNWS	ΔDEMP	ΔCNWS	ΔCSWS	MCNWS	ΔLogBLD
	1	1	0.75	0.75	0.5	0.5	0.5	0.5	0.25	0.25	0
Summer	Time dummies	ΔPRES	ΔLogBLD	ΔLogBLH	MCNWS	ΔDEMP	ΔCNWS	ΔTEMP	ΔLogHUMI	ΔCSWS	SNWS
	1	1	1	0.75	0.5	0.5	0.5	0.25	0.25	0.25	0
Autumn	Time dummies	ΔLogBLH	ΔTEMP	ΔPRES	ΔLogHUMI	ΔLogBLD	SNWS	ΔCSWS	MCNWS	ΔDEMP	ΔCNWS
	1	0.75	0.5	0.5	0.5	0.5	0.5	0.5	0.5	0.5	0.25
Winter	Time dummies	MCNWS	ΔPRES	ΔLogHUMI	ΔLogBLH	ΔLogBLD	SNWS	ΔCSWS	ΔTEMP	ΔDEMP	ΔCNWS
	1	1	0.75	0.75	0.5	0.5	0.5	0.5	0.25	0.25	0

variability in the selected meteorological variables for the selected short calm episodes. Despite the variability, the selected meteorological variables tended to have similar signs among the four site clusters as reported in Table S3.

The subsequent analyses are based on the selected variables under Model (4.1). Without causing confusion, the selected meteorological and pre-episode variables are denoted as ΔM_{ijt} and C_{ij}, respectively. Let $X_{ijt} = (\Delta M_{ijt}^\top, C_{ij}^\top, I_{ijt}^\top)^\top$ be the vector of selected covariates at time t for episode j in year i. The OLS estimator for θ_i is

$$\widehat{\theta}_i = \left(\sum_{j=1}^{n_i} \sum_{t=1}^{T_{ij}} X_{ijt} X_{ijt}^\top \right)^{-1} \sum_{j=1}^{n_i} \sum_{t=1}^{T_{ij}} X_{ijt} \Delta Y_{ijt}.$$

It is shown in the SI that under some assumptions, $\widehat{\theta}_i$ is unbiased and consistent for θ_i with the asymptotic normality. To estimate the variance of OLS estimator $\widehat{\theta}_i$ in the case of heteroskedastic and serial correlated errors $\{\varepsilon_{ijt}\}$, several robust variance estimators for panel data regression have been proposed (Arellano, 1987; Liang and Zeger, 1986; White, 1980). In consideration of the different lengths of the calm episodes we use the robust variance estimator

$$\widehat{\mathrm{Var}}\left(\widehat{\theta}_i\right) = \left(\sum_{j=1}^{n_i} \sum_{t=1}^{T_{ij}} X_{ijt} X_{ijt}^\top \right)^{-1} \left[\sum_{j=1}^{n_i} \left(\sum_{t=1}^{T_{ij}} X_{ijt} \widehat{\varepsilon}_{ijt} \right) \left(\sum_{t=1}^{T_{ij}} X_{ijt} \widehat{\varepsilon}_{ijt} \right)^\top \right] \left(\sum_{j=1}^{n_i} \sum_{t=1}^{T_{ij}} X_{ijt} X_{ijt}^\top \right)^{-1}, \tag{4.2}$$

where $\widehat{\varepsilon}_{ijt} = \Delta Y_{ijt} - X_{ijt}^\top \widehat{\theta}_i$ is the OLS residual.

4.2. Meteorological adjustment

As the meteorological variables are subject to yearly variations, we need to adjust for such variation in order to compare fairly the pollution growth characteristics within episodes among different years. Doing so would make the estimated growth rates within episodes reflect the local emission rather than the meteorological profiles. We extend the adjustment framework established in Liang et al. (2015) and Zhang et al. (2020) for the current episode-based analysis by constructing meteorological baseline distributions for each season and cluster.

As the calm episodes have different lengths, let n_{il} denote the number of episodes whose length is l hours for a site cluster and a season in year i. Let $U_{ijt} := (\Delta M_{ijt}^\top, C_{ij}^\top)^\top$ be the meteorological variables used in Model (4.1). We assume the episodes with the same length share the same meteorological distribution and define a set of positive probability weights $\{p_{il}\}_{l=3}^{\widetilde{T}_i}$ that adds up to one and is subject to $\frac{n_{il}}{n_i} \to p_{il}$ as $n_i \to \infty$ for any $3 \le l \le \widetilde{T}_i$ in a site cluster and a season of year i.

Let $f_{it}(u|l)$ be the conditional density of U_{ijt} given $T_{ij} = l$ for $t \le l$. Then, the density $f_{it}(u)$ of U_{ijt} at hour t in a site cluster and a certain season of year i is a mixture of the densities with different lengths of episodes not smaller than t, namely

$$f_{it}(u) = \left(\sum_{l \ge t} p_{il} \right)^{-1} \sum_{l \ge t} p_{il} f_{it}(u|l).$$

Let $\mu_{it}(\Delta m_{ijt}, c_{ij}) := \mathbb{E}(\Delta Y_{ijt} | \Delta M_{ijt} = \Delta m_{ijt}, C_{ij} = c_{ij}) = \Delta m_{ijt}^\top \beta_i + c_{ij}^\top \gamma_i + I_t^\top \eta_i$, where I_t is a $\widetilde{T}_i$ dimensional vector of which all elements are 0 except the t-th element equals 1. Then, the average concentration at hour t of the episode is

$$\mathbb{E}(\Delta Y_{ijt}) = \int \mu_{it}(u) f_{it}(u) du.$$

However, the above average based on the density $f_{it}(u)$ of year i is confounded by the meteorological condition of year i. A version that is free of the confounding is needed.

In consideration of the unbalanced data panels, we focus on the adjustment at hours $t = 1, \cdots, \min_{1 \le a \le A} \widetilde{T}_a$ so that the data of all A years can be utilised for the baseline meteorological construction. A solution to remove the yearly meteorological confounding is to replace $f_{it}(u)$ by an equally weighted density over A years:

$$f_{\cdot t}(u) = \frac{1}{A}\sum_{a=1}^{A} f_{at}(u) = \frac{1}{A}\sum_{a=1}^{A}\left(\sum_{l \ge t} p_{al}\right)^{-1} \sum_{l \ge t} p_{al} f_{at}(u|l), \tag{4.3}$$

which defines the baseline meteorological condition over the $A = 6$ years.

The adjusted average at time t in year i is the mean of ΔY_{ijt} for $U_{ijt} \sim f_{\cdot t}(u)$, that is

$$\mu_{it}^{*} = \int \mu_{it}(u) f_{\cdot t}(u) du = \frac{1}{A}\sum_{a=1}^{A}\left(\sum_{l \ge t} p_{al}\right)^{-1} \sum_{l \ge t} p_{al} \int \mu_{it}(u) f_{at}(u|l) du \tag{4.4}$$

$$= I_t^{\top}\eta_i + \frac{1}{A}\sum_{a=1}^{A}\left(\sum_{l \ge t} p_{al}\right)^{-1} \sum_{l \ge t} p_{al} \mathbb{E}\left(\Delta M_{ajt} | T_{aj} = l\right)^{\top} \beta_i$$

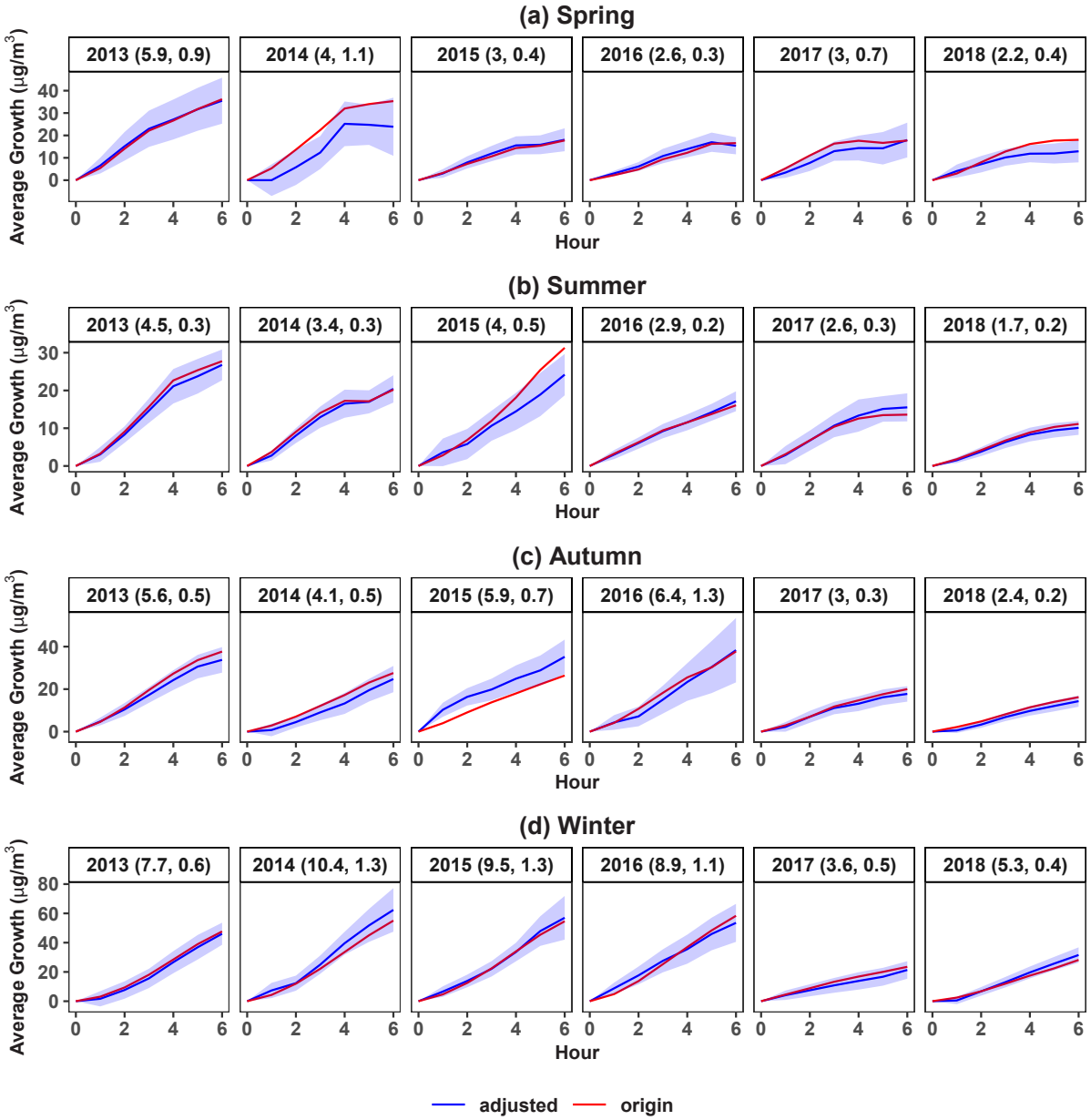

Fig. 3. The adjusted (blue) and original (red) average growth ($\mu g/m^3$) of $PM_{2.5}$ in the first 6 h of the calm episodes for cluster Beijing NW in (a) spring (b) summer (c) autumn and (d) winter of six years. The 95% confidence intervals of adjusted averaged change of $PM_{2.5}$ are indicated by shading. And the adjusted average growth rate ($\mu g/m^3$ per hour) in the first 6 h of the episodes that is the slope of the line between the first point and the last point on the curve of adjusted average growth as well as standard errors is marked in the parentheses. (For interpretation of the references to color in this figure legend, the reader is referred to the Web version of this article.)

$$+\frac{1}{A}\sum_{a=1}^{A}\left(\sum_{l\geq t}p_{al}\right)^{-1}\sum_{l\geq t}p_{al}\mathbb{E}\left(C_{aj}\middle|T_{aj}=l\right)^{\top}\gamma_i.$$

The meteorologically adjusted mean μ_{it}^{*} can be estimated by

$$\widehat{\mu}_{it}^{*}=I_t^{\top}\widehat{\eta}_i+\left(\frac{1}{A}\sum_{a=1}^{A}\frac{1}{\sum_{l\geq t}n_{al}}\sum_{s:T_{as}\geq t}\Delta M_{ast}^{\top}\right)\widehat{\beta}_i+\left(\frac{1}{A}\sum_{a=1}^{A}\frac{1}{\sum_{l\geq t}n_{al}}\sum_{s:T_{as}\geq t}C_{as}^{\top}\right)\widehat{\gamma}_i, \tag{4.5}$$

which makes the concentration during the calm episodes in different years comparable and reflects changes in the underlying emission.

In the SI, we provide the consistency, the asymptotic normality and the variance estimation of $\widehat{\mu}_{it}^{*}$ for any $i=1,\cdots,A$ and $\widehat{\mu}_{it}^{*}-\widehat{\mu}_{i't}^{*}$ for any $i\neq i'$ as $\min_{1\leq a\leq A}n_a\to\infty$ under some assumptions, which can be used to test if any two years' growth rates were the same or not. We choose the growth rate in the first T hours of the episodes μ_{iT}^{*}/T as the criterion to compare the pollution growth in different years.

5. Results and analyses

Using Model (4.1) with the selected variables and the meteorological adjustment approach, we obtain the within-episode growth patterns for $PM_{2.5}$, NO_2 and SO_2 in the four site clusters. The growth patterns reflect the local emission as the episodes are specially selected for that purpose. Fig. 3 displays the meteorologically adjusted growth curves $\widehat{\mu}_{it}^{*}$ with the 95% confidence intervals for the first 6 h of episodes in the four seasons

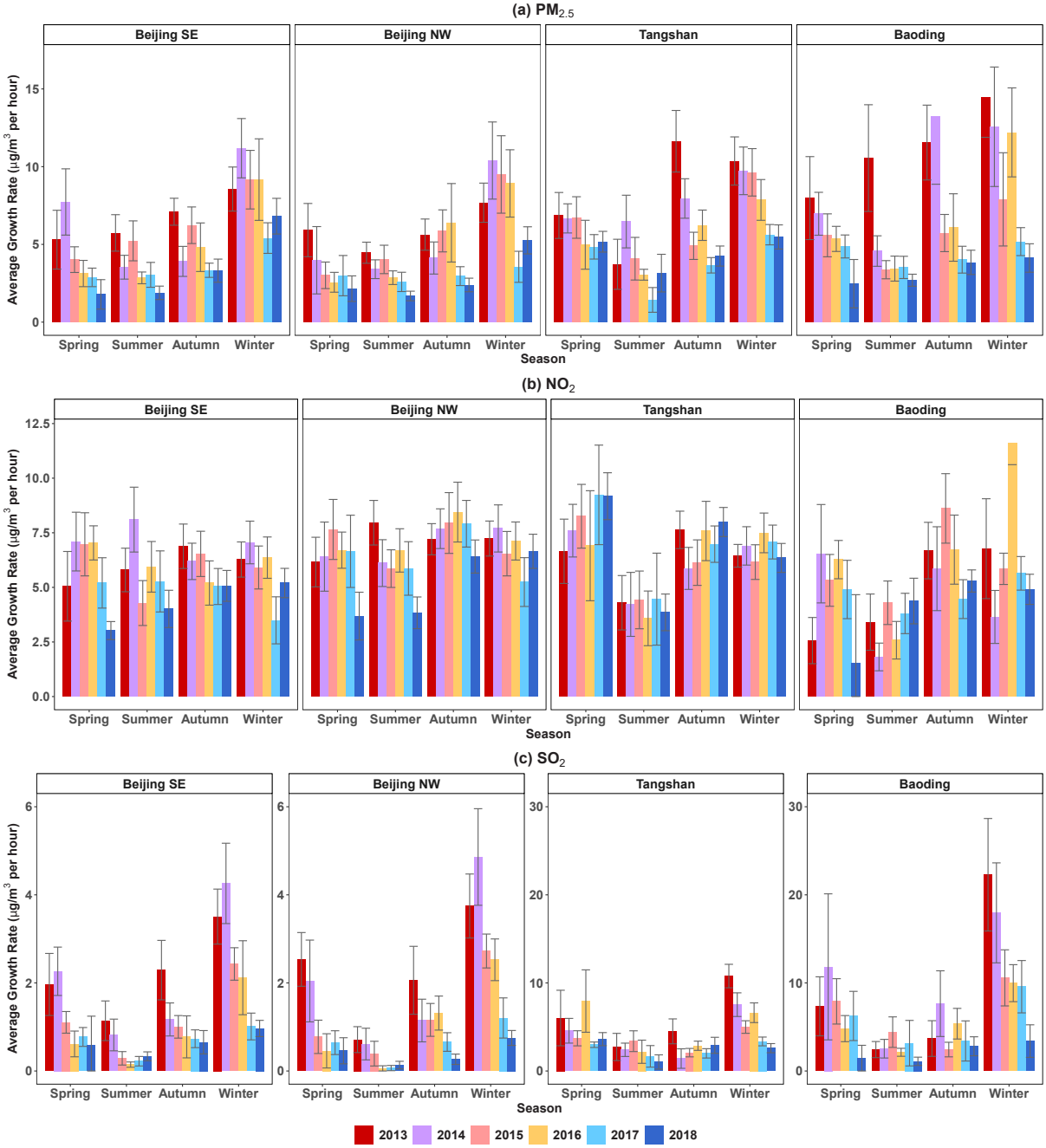

Fig. 4. The adjusted average growth rate ($\mu g/m^3$ per hour) of (a) $PM_{2.5}$, (b) NO_2 and (c) SO_2 in the first 6 h of the episodes for four clusters in four seasons of six seasonal years, 2013 (red), 2014 (purple), 2015 (pink), 2016 (yellow), 2017 (light blue), 2018 (blue) with the bars indicating the 95% confidence intervals. (For interpretation of the references to color in this figure legend, the reader is referred to the Web version of this article.)

of years 2013–2018 for Beijing NW. Figures for other site clusters and pollutants are provided in Figures S10–S20 of the SI. It is noted that the smallest 25%, 50% and 75% quantiles of the episode lengths among the four site clusters for each season (Table 1) were 4, 6 and 9 h, respectively. We chose the first 6 h to ensure at least half of the data being used to construct the growth curves and to build the baseline meteorological distributions. The raw growth curves by directly averaging the hourly concentrations of the episodes are also shown in Fig. 3. While most of the adjusted curves were close to the raw ones, there were occasions, for instance, spring of 2014 and 2018 and summer and fall of 2015, where the discrepancies between two curves for $PM_{2.5}$ were substantial. Figures S13 to S16 in the SI also displayed larger discrepancies for NO_2. The meteorological adjustment avoids the likely meteorological confounding. Fig. 3 and the similar figures in the SI display monotone growth in the episodes with increased volatility. In most situations, the growth pattern was largely linear in the early hours with some tapering off toward the 6 h cut-off.

Fig. 4 displays the average growth rates $\widehat{\mu}^{*}_{i6}/6$ ($\mu g/\ m^3$ per hour) within the first 6 h of the calm episodes for the three pollutants and the four site clusters. It shows different seasonal patterns in the local emission, with the growth rates in winter being the largest and those in the summer the smallest for $PM_{2.5}$ and SO_2, while the seasonal variation for NO_2 in Beijing was the least among the three cities. It also suggests temporal declines in the growth rates for $PM_{2.5}$ and SO_2 in all four seasons, with the most significant declines happened in winter in all four site clusters. The largest declines happened in winter 2017 for $PM_{2.5}$ and winter 2018 for SO_2 in Beijing, and in winter 2018 in Baoding for both $PM_{2.5}$ and SO_2. The declines in $PM_{2.5}$ and SO_2 were largely driven by a significant reduction in coal consumption and improvements in the coal combustion processes in North China. It is surprising to see that the winter growth rates of $PM_{2.5}$ in Beijing were comparable to those in the heavy industrial Tangshan and Baoding. Alarmingly, the 2018's winter $PM_{2.5}$ growth rate in Beijing SE was higher than its Hebei peers.

In contrast to the general reduction in local emission related to $PM_{2.5}$ and SO_2, there had been no significant reduction in NO_2 related emission in spring and winter in Baoding and Tangshan. Indeed, for all city clusters and seasons, no significant reduction in the growth rate of NO_2 occurred earlier than that of $PM_{2.5}$. A substantial portion of the Tangshan's NO_2 came from its huge steel making activities (91.2 million tonnes in 2017, accounting for more than 11% of China's and 5% of the world production), and its much lower NO_2 growth rate in summer reflects the annual cycle in the steel production. However, for non-summer seasons, the growth rates in Tangshan were quite similar to those in the two site clusters in Beijing, except being higher in 2017 and 2018. As Beijing has no major industrial activities, these suggest that Beijing's 5–6 million cars' emissions from 2013 to 2018 generated as much NO_2 as the 2 million vehicles plus the steel making activities in Tangshan. Beijing's NO_2 growth rates out-numbered those in Baoding in almost all seasons and years. These highlight the enormous contribution of Beijing's huge vehicle fleet for NO_x and then to $PM_{2.5}$ and O_3 generation.

The averages of adjusted average growth rates over four seasons for each year are listed in Table 4 which shows the annual meteorologically adjusted average hourly growth rates in 2018 relative to the 2013 levels in Beijing were reduced by 3.1 $\mu g/m^3$ (49.8%) for $PM_{2.5}$, 1.7 $\mu g/m^3$ (76.9%) for SO_2 and 1.8 $\mu g/m^3$ (27.9%) for NO_2. The reductions in Baoding were 7.8 $\mu g/m^3$ (70.5%) for $PM_{2.5}$, 6.7 $\mu g/m^3$ (75.6%) for SO_2 and 0.8 $\mu g/m^3$ (17.1%) for NO_2. The adjusted average hourly growth rates in Tangshan were reduced by 3.6 $\mu g/m^3$ (44.6%) for $PM_{2.5}$, 3.5 $\mu g/m^3$ (57.8%) for SO_2, but up by 0.6 (9.4%) for NO_2 in 2018.

Fig. 5 displays the difference series between the adjusted 6-h average growth rates of the three pollutants in 2014–2018 and those in 2013, which confirm the temporal patterns displayed in Fig. 4 and provides more detailed information on the timing and the extent of the temporal changes in the 6-h growth rates; Table S4 in the SI provides more details. For $PM_{2.5}$, the significant reduction in summer and fall mostly happened in 2014 in the four site clusters, with the exception in summer for Tangshan and fall for Baoding, which was delayed to 2017 and 2015, respectively. For spring, declines in the $PM_{2.5}$ growth rates took place for Beijing SE, Tangshan and Baoding in 2016, but earlier in 2015 for Beijing NW. For winter, the growth rates in two site clusters of Beijing started to reduce in 2017, while those in Tangshan and Baoding happened 1–2 years earlier. In summary, the declines in growth rates in $PM_{2.5}$ have been established for all seasons and all site clusters by 2017.

For all seasons except the winter in Beijing, the slowing down in the average growth rates of $PM_{2.5}$ over the levels in 2013 was extended in 2016–2017. However, in winter 2018, the slowing down was reversed by 1.4–1.7 $\mu g/m^3$ over the same period in 2017 in both site clusters in Beijing. The reduction in the growth rates of SO_2 as compared with those in 2013 was the most pronounced in winter with all four clusters started to see significant decline no later than 2015. Beijing was the earliest city that saw a significant reduction in spring and fall no later than 2015, while its summer decline came one year later in 2016 for Beijing NW. Baoding's SO_2 did not show a significant decrease from spring to fall before 2018. Tangshan faired better than Baoding for the SO_2 reduction, but the spring and summer reduction still came quite later. These show variation among the three cities in reducing the local emission related to the SO_2. However, the situation of NO_2 pollution was rather disappointing. A significant reduction in the spring and winter of Beijing did not happen before 2017. Tangshan's NO_2 growth actually increased over the 2013 level in recent years. The average reductions in both absolute and relative terms in the 6-h average growth rates in years 2014–2018 over those in 2013 are reported in Table S4, which supports the result in Fig. 4.

6. Discussion

In order to gauge the local emission, we construct an algorithm to

Table 4
The annual average of the adjusted average growth rates ($\mu g/m^3$ per hour) over four seasons from 2013 to 2018 with its (relative) reduction in 2018 with respect to 2013 and 2014. The negative value implies an increase.

Pollutant	Cluster	2013	2014	2015	2016	2017	2018	Reduction (to 2013)	Reduction (to 2014)
$PM_{2.5}$	Beijing SE	6.7	6.6	6.2	5	3.7	3.5	3.2 (48.3%)	3.1 (47.7%)
	Beijing NW	5.9	5.5	5.6	5.2	3	2.9	3 (51.5%)	2.6 (47.6%)
	Tangshan	8.1	7.7	6.3	5.5	3.9	4.5	3.6 (44.6%)	3.2 (41.4%)
	Baoding	11.1	9.3	5.6	6.8	4.4	3.3	7.8 (70.5%)	6 (64.8%)
NO_2	Beijing SE	6	7.1	5.9	6.1	4.8	4.3	1.7 (27.9%)	2.8 (39.2%)
	Beijing NW	7.1	7	7	7.2	6.4	5.1	2 (27.9%)	1.8 (26.2%)
	Tangshan	6.2	6.1	6.2	6.4	6.9	6.8	−0.6 (-9.4%)	−0.7 (-11.3%)
	Baoding	4.8	4.4	6	6.8	4.7	4	0.8 (17.1%)	0.4 (9.8%)
SO_2	Beijing SE	2.2	2.1	1.2	0.9	0.7	0.6	1.6 (71.5%)	1.5 (70.2%)
	Beijing NW	2.3	2.2	1.3	1.1	0.6	0.4	1.9 (82.2%)	1.8 (81.4%)
	Tangshan	6	4	3.5	4.9	2.5	2.5	3.5 (57.8%)	1.5 (36.2%)
	Baoding	8.9	10	6.3	5.6	5.6	2.2	6.7 (75.6%)	7.8 (78.2%)

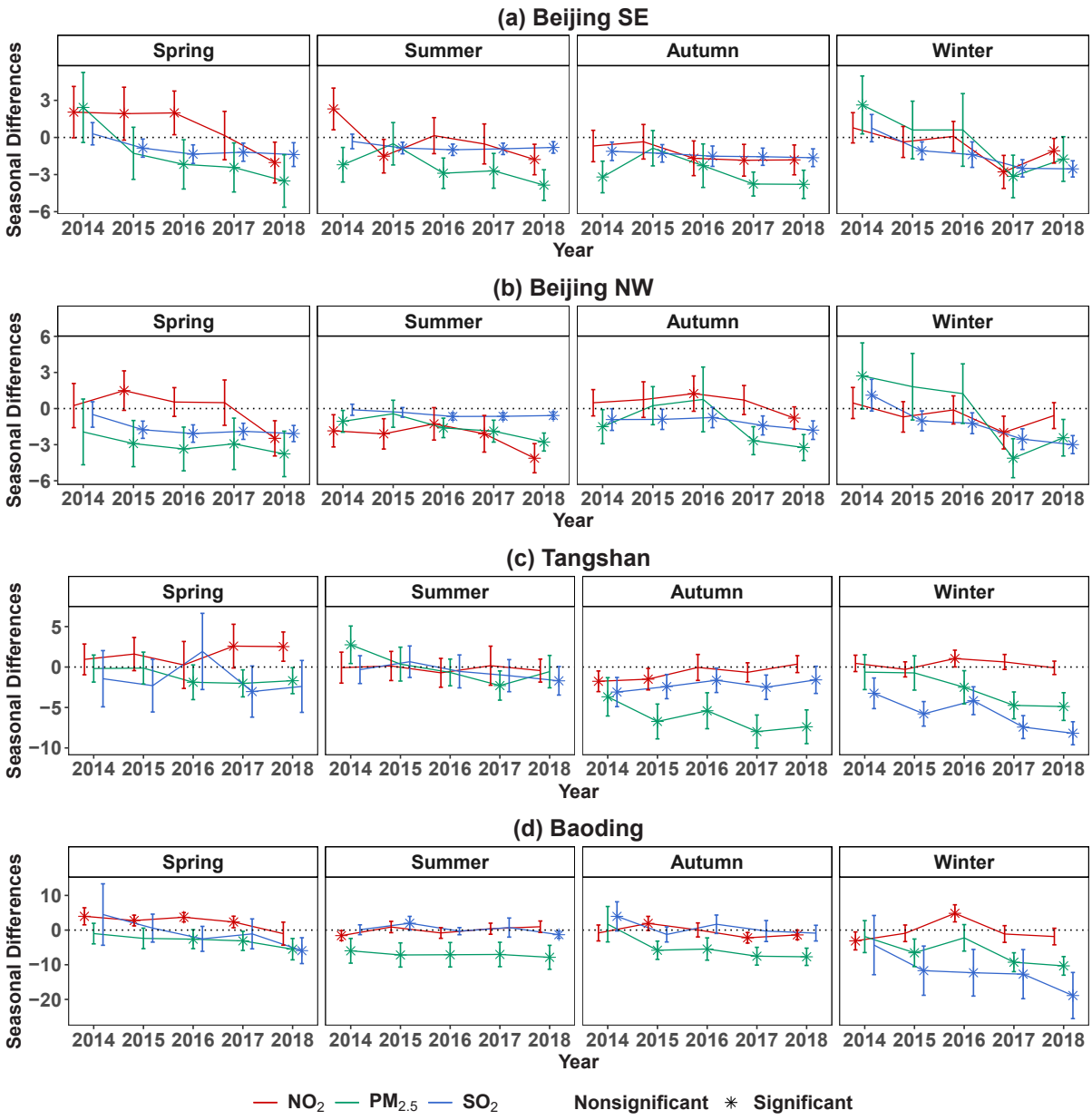

Fig. 5. Seasonal differences in the average adjusted growth rates ($\mu g/m^3$ per hour) of $PM_{2.5}$ (green), NO_2 (red) and SO_2 (blue) in the first 6 h of the calm episodes between years 2014–2018 and 2013 with the 95% confidence intervals. The significant (non-significant) differences away from zero at the 5% level with one-sided alternative are marked by asterisks (points), respectively. (For interpretation of the references to color in this figure legend, the reader is referred to the Web version of this article.)

distract calm episodes from monitoring concentration time series of three pollutants, which happened after sustained cleaning by the pollution-reducing wind to avoid regional transportation. The calm episode selection algorithm is much motivated by the geographical information in North China. The algorithm can be applied to other locations in the world by replacing the northerly vs southerly regimes corresponding to the air pollutants' removal and transportation with ones suitable to the particular location. The statistical model and analysis for estimating the growth rates would be the same. The output of our proposal, the average growth rates, are not emission inventory per se, but rather more timely measures that reflect the underlying emission, which may be used to adjust for the conventional EIs in finer temporal resolution.

Our results on the meteorologically adjusted growth rates of the three pollutants are consistent with some published results. For instance, de Foy et al. (2016) considered satellite retrieved NO_2 data via OMI and showed an increase in NO_2 concentration over 18 NO_2 hot-spot regions in China from 2005 to 2011, followed by a significant decrease till 2015. Although our study period only overlaps with de Foy et al.'s over 2013 to 2015 period, our results as summarized in Table 4 show Beijing's and Baoding's reduction in the NO_2's growth rates in 2018 relative to that in 2013 with an increase in NO_2 growth rate in Tangshan. Hua et al. (2021) investigated the holiday and weekend effects over the heating seasons in the greater Beijing region from 2014 to 2018 based on the ground monitoring data. It showed an annual reduction of 14% in NO_2 from 2014 to 2018 in the heating seasons. Our study as reported in Table S5 shows the adjusted average growth rates for NO_2 in 2018 relative to levels in 2014 in winter for the two site clusters in Beijing were 13.6% and 26.3% lower, respectively, which was consistent with the results in Hua et al. (2021). The slower progress on NO_2 emission control

compared with that SO_2 shown in our study also supports the revelation of an increased contribution of vehicle exhaust to $PM_{2.5}$ concentrations in the Beijing-Tianjin-Hebei region from 19% in March 2013 to 54% in March 2018 (Chen et al., 2019) and the findings in Huang et al. (2017); Liang et al. (2020). Figures S21–S24 demonstrate that our main conclusions are also in accordance with the trend of the official statistics on energy consumption, outputs of heavy industry products and the aggregated emission estimates released by Municipal Bureau of Statistics and NBS Survey Office in three cities since 2013. The declined growth rates in SO_2 and $PM_{2.5}$ were mostly the results of sustained effort in cleaner combustion of coal and the reduced domestic use of coal for cooking and winter heating over the NCP (Chen and Chen, 2019). The lack of reduction in the NO_2 growth rate reflects a dilemma that the three cities have been facing in controlling emissions from their ever increasing motor vehicle fleets. Clearly, the policies having been put in place in recent years to control motor vehicle emissions, which include making every domestic car off the road one day per working week and upgrading the fuel emission standards, are insufficient to cut back the NO_2 growth rates. The very subdued NO_2 situation explained the sustained O_3 rise in the NCP (Chen et al., 2018), which should encourage city authorities to unveil policies to reduce the growth rate of NO_2 that can lead to further decline in $PM_{2.5}$.

CRediT authorship contribution statement

Yuru Zhu: Conceptualization, Methodology, Software, Formal analysis, Data curation, Writing – original draft, Writing – review & editing, Validation. **Yinshuang Liang:** Investigation, Data curation, Formal analysis. **Song Xi Chen:** Conceptualization, Writing – original draft, Writing – review & editing, Supervision, Funding acquisition.

Declaration of competing interest

The authors declare that they have no known competing financial interests or personal relationships that could have appeared to influence the work reported in this paper.

Acknowledgment

The research was partially supported by China's National Key Research Special Program Grant 2016YFC0207701, National Natural Science Foundation of China Grants 92046021, 12026607, 12071013 and 71973005, Center for Statistical Science at Peking University; LMEQF at Peking University.

Appendix A. Supplementary data

Supplementary data to this article can be found online at https://doi.org/10.1016/j.atmosenv.2021.118323.

References

Arellano, M., 1987. Computing robust standard errors for within-groups estimators. Oxf. Bull. Econ. Stat. 49, 431–434. URL: https://ideas.repec.org/a/bla/obuest/v49y1987i4p431-34.html.

Baoding Municipal Bureau of Statistics, NBS Survey Office in Baoding, 2019. Baoding Economy Statistical Yearbook 2019. China Statistical Press, Beijing, China. URL: https://navi.cnki.net/KNavi/YearbookDetail?pcode=CYFD&pykm=YBDJJ&bh. (Accessed 12 October 2020).

Baoding Municipal Bureau of Statistics, NBS Survey Office in Baoding, 2020. Statistical communiqué on the national economy and social development of baoding in 2019. http://www.bd.gov.cn/zwgknr-888888008-235449.html. (Accessed 12 October 2020).

Beck, N., Katz, J.N., 1995. What to do (and not to do) with time-series cross-section data. Am. Polit. Sci. Rev. 89, 634–647. URL: http://www.jstor.org/stable/2082979.

Beijing Municipal Bureau of Statistics, Nbs Survey Office in Beijing, 2019. Beijing Statistical Yearbook 2019. China Statistical Press, Beijing, China. URL: http://nj.tjj.beijing.gov.cn/nj/main/2019-tjnj/zk/indexeh.htm. (Accessed 12 October 2020).

Beijing Municipal Bureau of Statistics, Nbs Survey Office in Beijing, 2020. Statistical CommuniquÃ© on the national economy and social development of beijing, 2019. http://tjj.beijing.gov.cn/EnglishSite/. (Accessed 12 October 2020).

Breusch, T.S., Pagan, A.R., 1979. A simple test for heteroscedasticity and random coefficient variation. Econometrica 47, 1287–1294. URL: http://www.jstor.org/stable/1911963.

Bun, R., Nahorski, Z., Horabik-Pyzel, J., Danylo, O., See, L., Charkovska, N., Topylko, P., Halushchak, M., Lesiv, M., Valakh, M., Kinakh, V., 2018. Development of a high-resolution spatial inventory of greenhouse gas emissions for Poland from stationary and mobile sources. Mitig. Adapt. Strategies Glob. Change 24, 853–880. https://doi.org/10.1007/s11027-018-9791-2.

Chen, H., Chen, W., 2019. Potential impact of shifting coal to gas and electricity for building sectors in 28 major northern cities of China. Appl. Energy 236, 1049–1061. https://doi.org/10.1016/j.apenergy.2018.12.051. URL: http://www.sciencedirect.com/science/article/pii/S0306261918318695.

Chen, L., Guo, B., Huang, J., He, J., Wang, H., Zhang, S., Chen, S.X., 2018. Assessing air-quality in Beijing-Tianjin-Hebei region: the method and mixed tales of PM2.5 and O3. Atmospheric Environment 193 290–301. URL: http://www.sciencedirect.com/science/article/pii/S1352231018305685.

Chen, Z., Chen, D., Wen, W., Zhuang, Y., Kwan, M.P., Chen, B., Zhao, B., Yang, L., Gao, B., Li, R., Xu, B., 2019. Evaluating the "2+26" regional strategy for air quality improvement during two air pollution alerts in Beijing: variations in $PM_{2.5}$ concentrations, source apportionment, and the relative contribution of local emission and regional transport. Atmos. Chem. Phys. 19, 6879–6891. https://doi.org/10.5194/acp-19-6879-2019. URL: https://acp.copernicus.org/articles/19/6879/2019/.

de Foy, B., Lu, Z., Streets, D.G., 2016. Satellite NO2 retrievals suggest China has exceeded its NOx reduction goals from the twelfth Five-Year Plan. Sci. Rep. 6, 35912. https://doi.org/10.1038/srep35912.

Gurney, K.R., Razlivanov, I., Song, Y., Zhou, Y., Benes, B., Abdul-Massih, M., 2012. Quantification of fossil fuel CO2 emissions on the building/street scale for a large U. S. city. Environ. Sci. Technol. 46, 12194–12202. https://doi.org/10.1021/es3011282.

Hastie, T., Tibshirani, R., Friedman, J., 2008. The Elements of Statistical Learning: Data Mining, Inference, and Prediction, 2 ed. Springer, pp. 58–60 (chapter 3).

Hua, J., Zhang, Y., de Foy, B., Mei, X., Shang, J., Feng, C., 2021. Competing PM2.5 and NO2 holiday effects in the Beijing area vary locally due to differences in residential coal burning and traffic patterns. Science of The Total Environment 750 141575. https://doi.org/10.1016/j.scitotenv.2020.141575. URL: https://www.sciencedirect.com/science/article/pii/S0048969720351044.

Huang, K., Zhuang, G., Wang, Q., Fu, J.S., Lin, Y., Liu, T., Han, L., Deng, C., 2014. Extreme haze pollution in Beijing during January 2013: chemical characteristics, formation mechanism and role of fog processing. Atmos. Chem. Phys. Discuss. 14, 7517–7556. https://doi.org/10.5194/acpd-14-7517-2014. URL: https://www.atmos-chem-phys-discuss.net/14/7517/2014/.

Huang, T., Zhu, X., Zhong, Q., Yun, X., Meng, W., Li, B., Ma, J., Zeng, E.Y., Tao, S., 2017. Spatial and temporal trends in global emissions of nitrogen oxides from 1960 to 2014. Environ. Sci. Technol. 51, 7992–8000. https://doi.org/10.1021/acs.est.7b02235 arXiv.

Huang, Y., Shen, H., Chen, Y., Zhong, Q., Chen, H., Wang, R., Shen, G., Liu, J., Li, B., Tao, S., 2015. Global organic carbon emissions from primary sources from 1960 to 2009. Atmos. Environ. 122, 505–512. https://doi.org/10.1016/j.atmosenv.2015.10.017. URL: http://www.sciencedirect.com/science/article/pii/S1352231015304362.

Kunik, L., Mallia, D., Gurney, K., Mendoza, D., Oda, T., Lin, J., 2019. Bayesian inverse estimation of urban CO2 emissions: results from a synthetic data simulation over Salt Lake City, UT. Elem Sci Anth 7, 36. https://doi.org/10.1525/elementa.375.

Lee, S.M., Princevac, M., Mitsutomi, S., Cassmassi, J., 2009. MM5 simulations for air quality modeling: an application to a coastal area with complex terrain. Atmos. Environ. 43, 447–457. https://doi.org/10.1016/j.atmosenv.2008.07.067. URL: http://www.sciencedirect.com/science/article/pii/S1352231008006614.

Li, X., Zhang, Q., Zhang, Y., Zheng, B., Wang, K., Chen, Y., Wallington, T.J., Han, W., Shen, W., Zhang, X., He, K., 2015. Source contributions of urban PM2.5 in the Beijing-Tianjin-Hebei region: changes between 2006 and 2013 and relative impacts of emissions and meteorology. Atmos. Environ. 123, 229–239. https://doi.org/10.1016/j.atmosenv.2015.10.048. URL: http://www.sciencedirect.com/science/article/pii/S1352231015304660.

Liang, C.S., Wu, H., Li, H.Y., Zhang, Q., Li, Z., He, K.B., 2020. Efficient data preprocessing, episode classification, and source apportionment of particle number concentrations. Sci. Total Environ. 744, 140923. https://doi.org/10.1016/j.scitotenv.2020.140923. URL: http://www.sciencedirect.com/science/article/pii/S0048969720344521.

Liang, K.Y., Zeger, S.L., 1986. Longitudinal data analysis using generalized linear models. Biometrika 73, 13–22. URL: http://www.jstor.org/stable/2336267.

Liang, X., Zou, T., Guo, B., Li, S., Zhang, H., Zhang, S., Huang, H., Chen, S.X., 2015. Assessing Beijing's PM2.5 pollution: severity, weather impact, APEC and winter heating. Proc. Math. Phys. Eng. Sci. 471, 20150257. https://doi.org/10.1098/rspa.2015.0257. URL: https://royalsocietypublishing.org/doi/abs/10.1098/rspa.2015.0257.

Mep, 2017. 2017 air pollution prevention and management plan for the Beijing-Tianjin-Hebei region and its surrounding areas. http://dqhj.mee.gov.cn/dtxx/201703/t20170323_408663.shtml. (Accessed 12 October 2020).

Nickless, A., Rayner, P.J., Engelbrecht, F., Brunke, E.G., Erni, B., Scholes, R.J., 2018. Estimates of CO2 fluxes over the city of Cape Town, South Africa, through Bayesian inverse modelling. Atmos. Chem. Phys. 18, 4765–4801. https://doi.org/10.5194/acp-18-4765-2018. URL: https://acp.copernicus.org/articles/18/4765/2018/.

Seo, J., Kim, J.Y., Youn, D., Lee, J.Y., Kim, H., Lim, Y.B., Kim, Y., Jin, H.C., 2017. On the multiday haze in the Asian continental outflow: the important role of synoptic conditions combined with regional and local sources. Atmos. Chem. Phys. 17, 9311–9332. https://doi.org/10.5194/acp-17-9311-2017. URL: https://acp.copernicus.org/articles/17/9311/2017/.

Su, T., Li, J., Li, C., Lau, A.K.H., Yang, D., Shen, C., 2017. An intercomparison of AOD-converted PM2.5 concentrations using different approaches for estimating aerosol vertical distribution. Atmos. Environ. 166, 531–542. https://doi.org/10.1016/j.atmosenv.2017.07.054. URL: http://www.sciencedirect.com/science/article/pii/S1352231017305034.

Su, T., Li, Z., Kahn, R., 2018. Relationships between the planetary boundary layer height and surface pollutants derived from lidar observations over China: regional pattern and influencing factors. Atmos. Chem. Phys. 18, 15921–15935. https://doi.org/10.5194/acp-18-15921-2018.

Tangshan Municipal Bureau of Statistics, NBS Survey Office in Tangshan, 2020a. Statistical communiqué on the national economy and social development of tangshan in 2019. http://new.tangshan.gov.cn/zhengwu/tjxx/20200403/909974.html. (Accessed 12 October 2020).

Tangshan Municipal Bureau of Statistics, NBS Survey Office in Tangshan, 2020b. Tangshan Statistical Yearbook 2019. China Statistical Press, Beijing, China. URL: http://new.tangshan.gov.cn/zhengwu/tjxx/20200519/909919.html. (Accessed 12 October 2020).

Tie, X., Madronich, S., Li, G., Ying, Z., Zhang, R., Garcia, A.R., Lee-Taylor, J., Liu, Y., 2007. Characterizations of chemical oxidants in Mexico City: a regional chemical dynamical model (wrf-chem) study. Atmos. Environ. 41, 1989–2008. https://doi.org/10.1016/j.atmosenv.2006.10.053. URL: http://www.sciencedirect.com/science/article/pii/S1352231006010399.

Titov, M., Sturman, A.P., Zawar-Reza, P., 2007. Application of MM5 and CAMx4 to local scale dispersion of particulate matter for the city of Christchurch, New Zealand. Atmos. Environ. 41, 327–338. https://doi.org/10.1016/j.atmosenv.2006.08.012. URL: http://www.sciencedirect.com/science/article/pii/S1352231006008296.

Turnbull, J.C., Karion, A., Davis, K.J., Lauvaux, T., Miles, N.L., Richardson, S.J., Sweeney, C., McKain, K., Lehman, S.J., Gurney, K.R., Patarasuk, R., Liang, J., Shepson, P.B., Heimburger, A., Harvey, R., Whetstone, J., 2019. Synthesis of urban CO2 emission estimates from multiple methods from the Indianapolis Flux Project (INFLUX). Environ. Sci. Technol. 53, 287–295. https://doi.org/10.1021/acs.est.8b05552.

Wang, L., Zhang, N., Liu, Z., Sun, Y., Ji, D., Wang, Y., 2014a. The influence of climate factors, meteorological conditions, and boundary-layer structure on severe haze pollution in the Beijing-Tianjin-Hebei region during January 2013. Advances in Meteorology 1–14. https://doi.org/10.1155/2014/685971, 2014.

Wang, L.T., Wei, Z., Yang, J., Zhang, Y., Zhang, F.F., Su, J., Meng, C.C., Zhang, Q., 2014b. The 2013 severe haze over southern Hebei, China: model evaluation, source apportionment, and policy implications. Atmos. Chem. Phys. 14, 3151–3173. https://doi.org/10.5194/acp-14-3151-2014. URL: https://acp.copernicus.org/articles/14/3151/2014/.

Wang, Z., Li, J., Wang, Z., Yang, W., Tang, X., Ge, B., Yan, P., Zhu, L., Chen, X., Chen, H., Wand, W., Li, J., Liu, B., Wang, X., Zhao, Y., Lu, N., Su, D., 2014c. Modeling study of regional severe hazes over mid-eastern China in January 2013 and its implications on pollution prevention and control. Sci. China Earth Sci. 57, 3–13. https://doi.org/10.1007/s11430-013-4793-0.

White, H., 1980. A heteroskedasticity-consistent covariance matrix estimator and a direct test for heteroskedasticity. Econometrica 48, 817–838. URL: http://www.jstor.org/stable/1912934.

Wooldridge, J.M., 2010. Econometric Analysis of Cross Section and Panel Data, 2 ed., vol. 10. The MIT Press, The MIT Press, pp. 299–300.

Wu, D., Fung, J.C.H., Yao, T., Lau, A.K.H., 2013. A study of control policy in the Pearl River Delta region by using the particulate matter source apportionment method. Atmos. Environ. 76, 147–161. https://doi.org/10.1016/j.atmosenv.2012.11.069. URL: http://www.sciencedirect.com/science/article/pii/S1352231012011569.

Xing, J., Wang, S.X., Jang, C., Zhu, Y., Hao, J.M., 2011. Nonlinear response of ozone to precursor emission changes in China: a modeling study using response surface methodology. Atmos. Chem. Phys. 11, 5027–5044. https://doi.org/10.5194/acp-11-5027-2011. URL: https://acp.copernicus.org/articles/11/5027/2011/.

Xu, Z., Chen, S.X., Wu, X., 2020. Meteorological change and impacts on air pollution: results from North China. J. Geophys. Res.: Atmosphere 125. https://doi.org/10.1029/2020JD032423 e2020JD032423. URL: https://agupubs.onlinelibrary.wiley.com/doi/abs/10.1029/2020JD032423. arXiv:https://agupubs.onlinelibrary.wiley.com/doi/pdf/10.1029/2020JD032423.

Yang, K., Dickerson, R.R., Carn, S.A., Ge, C., Wang, J., 2013. First observations of SO2 from the satellite Suomi NPP OMPS: widespread air pollution events over China. Geophys. Res. Lett. 40, 4957–4962. https://doi.org/10.1002/grl.50952. URL: https://agupubs.onlinelibrary.wiley.com/doi/abs/10.1002/grl.50952. arXiv: https://agupubs.onlinelibrary.wiley.com/doi/pdf/10.1002/grl.50952.

Zhang, S., Chen, S., Guo, B., Wang, H., Lin, W., 2020. Regional air-quality assessment that adjusts for meteorological confounding. SCIENTIA SINICA Mathematica 50, 527. https://doi.org/10.1360/SCM-2019-0368.

Zhang, S., Guo, B., Dong, A., He, J., Xu, Z., Chen, S., 2017. Cautionary tales on air-quality improvement in Beijing. Proc. Math. Phys. Eng. Sci. 473, 20170457. https://doi.org/10.1098/rspa.2017.0457.

Zheng, G.J., Duan, F.K., Su, H., Ma, Y.L., Cheng, Y., Zheng, B., Zhang, Q., Huang, T., Kimoto, T., Chang, D., Pöschl, U., Cheng, Y.F., He, K.B., 2015. Exploring the severe winter haze in Beijing: the impact of synoptic weather, regional transport and heterogeneous reactions. Atmos. Chem. Phys. 15, 2969–2983. https://doi.org/10.5194/acp-15-2969-2015. URL: https://acp.copernicus.org/articles/15/2969/2015/.